CRACKING BEHAVIOR AND CRACK WIDTH PREDICTIONS OF FRP STRENGTHENED RC MEMBERS UNDER TENSION

Abstract

This paper presents and discusses the experimental results of uniaxial tensile tests of fiber reinforced polymer externally strengthened reinforced concrete (FRP strengthened RC) prisms in terms of crack width and crack spacing. As a non-contact and material independent system for in-time measurement of displacement and strain, the digital image correlation (DIC) technique has been used in this study for investigating the evolution of strains and formation of cracks during uniaxial tensile tests. As a result, the cracks were measured precisely at any load stage.

The experimental results of tests performed by authors and other researchers on FRP strengthened RC members in tension are compared to prediction models from code provisions and guidelines (Eurocode 2 and *fib* 14), and their suitability are analyzed and discussed. The results show the dependence of the behavior and crack characteristics of FRP strengthened RC members to parameters such as wrapping scheme and FRP reinforcement ratios which are not included in design provisions for crack analysis. A new formulation for crack width and spacing for FRP strengthened RC members, calibrated using the experimental results, has been proposed which considers all the main affecting parameters.

1. Introduction

As a response to corrosion problems in reinforcing steel, to enhance the durability of RC structures, and to increase the efficiency of strengthening systems, FRP composites became popular in civil engineering during the last three decades. Although the use of externally bonded

FRP composites is by now a recognized technique, some aspects of the ultimate and serviceability limit states needs further experimental and analytical investigations; especially for serviceability conditions, which there is a lack of design provisions. The serviceability design of FRP strengthened RC structures may be affected by the mechanical and bond properties of the additional external FRP reinforcement. Therefore, accurate modeling of the cracking and deformability behavior in such members is crucial. For FRP strengthened RC members the cracking behavior is typically evaluated by using the same approach used for RC members [1]. For the design, both the ultimate limit state and the serviceability limit state of the structure must be verified. An FRP strengthened RC member is designed for the required strength and afterwards checked for serviceability and the ultimate state criteria. It should be noted that in many cases, the serviceability criteria controls the design. According to clause 10.2.8 of ACI 440.2R-08 [2], to avoid inelastic deformations in FRP strengthened RC members at serviceability limit states, the stress in steel reinforcement should be limited to 80% of the yield strength.

Compared to the large numbers of experimental results on FRP strengthened RC elements which aim at studying the behavior at the ultimate stage, fewer results are available for verification of serviceability conditions under direct tension [1, 3-10]. Moreover, increase in the ultimate capacity due to FRP strengthening will not necessarily result in a proportional increase in the service load [1]; therefore, verification of serviceability limit state in FRP strengthened RC elements is crucial. A number of experimental tests have been conducted to evaluate the cracking of FRP strengthened RC flexural elements [11-13]. However, the behavior of FRP strengthened RC members under direct tension was the focus of few research studies [3-9].

In the case of RC structures, reliable and effective models are available for evaluating deflections and crack widths at the serviceability limit state, which also takes into account the tension stiffening effect [1]. The modelling of tension stiffening in RC beams is typically based on several experimental tests on specimens in uniaxial tension and bending. The code formulas are advanced by now for RC members. Also, studies related to members strengthened with FRP rods are progressing [14, 15]. However, for RC members strengthened by externally bonded FRP, the serviceability in terms of crack characteristics has not been well established; in this case further studies are needed regarding the transfer of stresses at the concrete-FRP interface, and also the interaction of the external reinforcement with internal steel. Limited research studies have investigated the crack characteristics and tension stiffening of externally bonded FRP strengthened prisms and beams [1, 3-10]. Some design provisions provide equations for calculating crack width and spacing for RC elements at serviceability conditions [16-21]. However, fewer provision are available for the serviceability conditions and crack width and spacing predictions in design codes for FRP strengthened RC structures. An available code formula for the prediction of mean crack spacing and width is presented in *fib* Bulletin 14 [21], which is based on the work presented by Matthys [8].

Applying FRP reinforcement significantly changes the crack width and spacing of the RC member, since tension stiffening phenomena develops both at the steel-concrete interface and the FRP-concrete interface. Therefore, average crack widths are generally smaller than for un-strengthened members at the same smeared strain level, due to the additional tension stiffening of the external FRP reinforcement developing at the FRP-concrete interface which reduces the crack spacing [3-10].

This paper presents and discusses the experimental results of FRP strengthened RC members tested under uniaxial tension. The tensile RC members (prisms) were reinforced with externally bonded FRP sheets. The prisms had different steel and FRP reinforcement ratios combined with different wrapping schemes. Details of the tensile behavior and also the crack characteristic analysis of the specimens are presented. The experimental results of tests performed by authors and results available in the literature on RC elements externally strengthened with FRP [4, 8, and 9] in terms of crack spacing and crack width are compared with code provisions and the suitability of the prediction models is analyzed. Finally, a new formulation for crack width and spacing for FRP strengthened RC members, calibrated using the experimental results, has been proposed which considers all the main affecting parameter.

The crack characteristics including crack width, number of cracks, and spacing are monitored by using a digital image correlation (DIC) system at the conducted experiments. The evolution of strains and deformations on FRP and concrete have been measured with a DIC system and its tracking method. This method has been widely used for measurements in RC members [22-25].

2. Principles of the cracking phenomena

If a continuously increasing tension load is applied to a member, the first crack will form when the tensile strength of the weakest section in the member is reached. This crack will result in a local redistribution of stress in that member. At the crack, all the tensile force will be transferred to the reinforcements, and the stress in the concrete adjacent to the crack will drop to zero [26]. With increasing distance from the crack, force is transferred from the reinforcements to the concrete by bond stress until, at some distance, S_0, from the crack; the stress distribution within the section remains unchanged from what it was before the crack formed. This local redistribution of forces in the region of the crack is accompanied by an extension of the member.

This extension, plus a minor shortening of the concrete which has been relieved of the tensile stress it was supporting, is accommodated in the crack. The crack thus opens up to a finite width immediately on its formation. The formation of the crack and the resulting extension of the member also reduce the stiffness of the member. As further load is applied, a second crack will form at the next weakest section, though it will not form within S_0 of the first crack since the stresses in this region will have been reduced by the formation of the first crack. However, if the second crack is formed at a distance more than $2S_0$ away from the first crack, there is a certain length between the two cracks where the concrete stress reaches the concrete tensile strength. This means at least one crack will form between two existing cracks if they are at a distance more than $2S_0$ apart. Further increase in load will lead to the formation of more cracks until there is no remaining area of the member surface which is not within S_0 of a previously formed crack. Further loading will result in widening of existing cracks but no new cracks will form, therefore a stable crack pattern with a crack spacing of S $(S_0 \leq S \leq 2S_0)$ is achieved. The variation of steel, concrete and FRP strains between two adjacent cracks are shown in Fig.1. Steel strain (ε_s) and FRP strain (ε_f) reduces from a peak at the crack location to a minimum halfway between the cracks; the concrete strain (ε_c) follows a converse pattern. It is assumed that the strain in FRP and steel at the crack location are the same (ε_{s0}). Since the bond stress between steel and concrete is not the same for FRP and concrete, with the increase of distance from the crack the strain variation of FRP and steel differ from each other, In Fig. 1, ε_{sm} and ε_{cm} are the average steel strain and average concrete strain. In RC members, the crack opening is computed as the integral of the difference between the steel and concrete strains over two half crack spacing (Fig.1.).

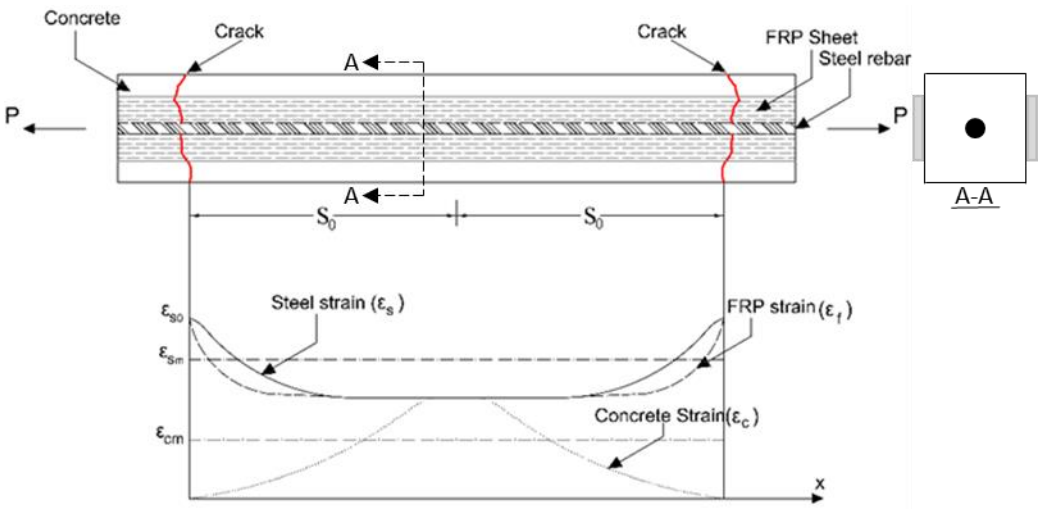

Fig.1. Schematic of strain distribution after cracks are formed

The distance S_0 of an existing crack, defines the average spacing of the cracks and the maximum spacing is $2S_0$. It is in the calculation of S_0 that the most significant differences arise between the equations in code provisions. The distance S_0 depends on the rate at which the stress can be transferred from the reinforcements, which are carrying all the force at a crack, to the concrete. This transfer is affected by bond stresses on the reinforcements. It is assumed that the bond stress is constant along the length S_0, and the stress will reach the tensile strength of the concrete at a distance S_0 from a crack.

2.1. Code provisions for crack spacing and crack width

The integrity of a structure is affected by the crack characteristics and therefore careful considerations should be made [27-28].In the past, tremendous amount of effort has gone into developing methods to predict the crack width and spacing in RC members and many equations have been proposed in different formats. A summary of the previous work on crack width and spacing formulations in RC members are presented in Borosnyoi and Balazs [29]. In general, these equations have the following format [30]:

$$w = k\varepsilon\left(\frac{d_b}{\rho}\right)$$

(1)

Where w is the average crack width. From the equation it can be seen that the key elements which affect the crack width are the bond characteristic parameter k, the bar diameter d_b, the reinforcement ratio ρ, and the average strain ε.

In Eurocode 2 [16], it is assumed that all the deformation of the member when a crack is formed is accommodated in that crack. When all cracks have formed, the crack width is given by the following relationship, which is based on compatibility:

$$w_k = \beta_k S_{rm} \varepsilon_{sm}$$

(2)

Where, w_k is the average crack width, β_k may be taken as 1.7 for load induced cracking, S_{rm} is the average crack spacing and ε_{sm} is the average strain. As shown in Eq. (3), in the crack width formulation given in EC2-04 [17], the average strain is assumed to be equal to the average strain in the reinforcements, ε_{sm}, taking account of tension stiffening, and taking out the average strain in the concrete at the surface, ε_{cm} (Fig.1).

$$w_k = \beta_k S_{rm}\left(\varepsilon_{sm} - \varepsilon_{cm}\right)$$

(3)

The following equation has been presented in EC2-92 [16] for average crack spacing:

$$S_{rm} = 50 + 0.25 k_1 k_2 \frac{\phi}{\rho_{eff}}$$

(4)

Where, k_1 is the bond coefficient equal to 0.8 for deformed bars and 1.6 for plain bars; k_2 is the coefficient to take into account the type of loading equal to 0.5 for bending and 1.0 for pure tension; $\emptyset$ is the diameter of steel bar; and ρ_{eff} is the effective reinforcement ratio.

More recent studies have shown that the cover of concrete also has a significant influence [30-32]. In EC2-04 [17] the following equation was proposed to evaluate the maximum crack spacing for RC elements:

$$S_{r,\max} = 3.4c + 0.425k_1k_2\frac{\phi}{\rho_{eff}} \tag{5}$$

Where c is the concrete cover and k_1, k_2, $\emptyset$, and ρ_{eff} are defined same as EC2-92 [16]. It was found experimentally that a reasonable estimate of the characteristic crack width is obtained if the maximum crack spacing is assumed to be 1.7 times the average crack spacing [17]. Therefore, based on EC2-04, the average crack spacing, S_{rm}, can be calculated as follows:

$$S_{rm} = 2c + 0.25k_1k_2\frac{\phi}{\rho_{eff}} \tag{6}$$

Ceroni [1] proposed the following expression for the effective reinforcement ratio to consider the effect of externally bonded FRP in Eurocode 2 equations:

$$\rho_{eff} = \frac{A_s + A_f E_f / E_s}{A_{c,eff}} \tag{7}$$

Where A_s is the area of steel reinforcement, A_f is the area of the FRP reinforcement, E_f and E_s are the Young's modulus of FRP and steel respectively. Also, $A_{c,eff}$ is the effective area of concrete in tension, reasonably assumed as an area surrounding the steel rebar with a radius of three times the diameter of the rebar.

In *fib* 14 [21], the average crack spacing in RC members strengthened with FRP sheets, taking into effect of both the internal and the external reinforcement, is calculated using the following formulation:

$$S_{rm} = \frac{2 f_{ctm} A_{c,eff}}{\tau_{sm} u_s} \frac{E_s A_s}{E_s A_s + \xi_b E_f A_f} = \frac{2 f_{ctm} A_{c,eff}}{\tau_{fm} u_f} \frac{\xi_b E_f A_f}{E_s A_s + \xi_b E_f A_f} \quad (8)$$

Where f_{ctm} is the mean tensile strength of concrete, u_s and u_f are the perimeters of the steel bar and FRP sheets bonded to concrete, τ_{fm}=1.8f_{ctm} [33] and τ_{sm}=1.25f_{ctm} [8] are the bond stresses along the concrete-steel interface and concrete-FRP interfaces, which are assumed constant and ξ_b is a bond parameter given as:

$$\xi_b = \frac{\tau_{fm} E_s A_s u_f}{\tau_{sm} E_f A_f u_s} \quad (9)$$

The other parameter in the crack width equation is the average strain. In EC2-92 [16], ε_{sm} is defined as:

$$\varepsilon_{sm} = \varepsilon_2 \left(1 - \beta_1 \beta_2 \left(\frac{\sigma_{cr}}{\sigma_s} \right)^2 \right) \quad (10)$$

Where β_1 considers the bond characteristics of the internal steel rebars (1 for ribbed and 0.5 for smooth bars), β_2 considers the loading type (1 for short and 0.5 for long term loading); σ_{cr} is the tensile stress in the steel bar at the first cracking load, σ_s and ε_2 are the stress and strain in the steel bar at the cracked section.

In EC2-04 [17] a different form of the equation is adopted and the difference in materials strains between cracks is described as:

$$\varepsilon_{sm} - \varepsilon_{cm} = \frac{\sigma_s}{E_s} - \frac{k_t f_{ctm}\left(1+\alpha_e \rho_{eff}\right)}{E_s \rho_{eff}} \geq 0.6\frac{\sigma_s}{E_s}$$

(11)

Where σ_s , is the stress in the tension reinforcement, calculated by assuming a cracked section, α_e is the modular ratio (E_s/E_c), k_t is a factor depending on the duration of the load (0.6 for short-term loads and 0.4 for long-term loads), and ρ_{eff} for FRP strengthened RC members is calculated as shown in Eq. (7).

In *fib*14 [21], the same approach as EC2-92 [16] is used for calculation of the average strain and average crack widths. By assuming that the initial strain at the extreme tensile fiber before strengthening is zero, ε_2 can be calculated as follows:

$$\varepsilon_2 = \frac{P_s + P_f}{E_s A_s + E_f A_f}$$

(12)

Where, P_s and P_f are the total tensile force in steel and FRP respectively.

3. Experimental program

In order to evaluate the behavior of FRP strengthened RC elements under tension, and to investigate the serviceability conditions, a series of full-scale tensile tests of FRP strengthened RC prisms have been conducted. The experimental program consisting thirteen full-scale FRP strengthened RC prisms tested under direct tensile loading was discussed in detail in [34-35]. Only a brief summary of the work and the main data are presented here. The test setup and dimensions of the specimens are shown in Fig. 2. The specimens are 1400 mm long RC prisms with a cross section of 257 mm × 178 mm. FRP sheets with a width of 200 mm were applied on the two opposite wider sides of the specimen. Pin connection was used at the ends to eliminate

any potential bending effect and ensure pure uniaxial loading. Three different wrapping schemes were used, including Side Bond (SB), Fully Wrapped (FW) and U-wrap with FRP Anchors (FA). Testing initially started using load control up to the first cracking and then switched to displacement control until failure of the specimen.

In Table 1, the material properties are reported; f_y and E_s being the yielding stress and Young's modulus of steel, respectively, t, $F_{u,FRP}$ and E_f are the thickness, ultimate strength and Young's modulus of FRP, respectively. In table 2, the steel bar diameter, d_b (Ø), internal steel reinforcement ratio, ρ_s, external FRP reinforcement ratio, ρ_f, the effective reinforcement ratio, ρ_{eff}, defined previously, of the tested specimens are reported.

a) North view of the test specimen

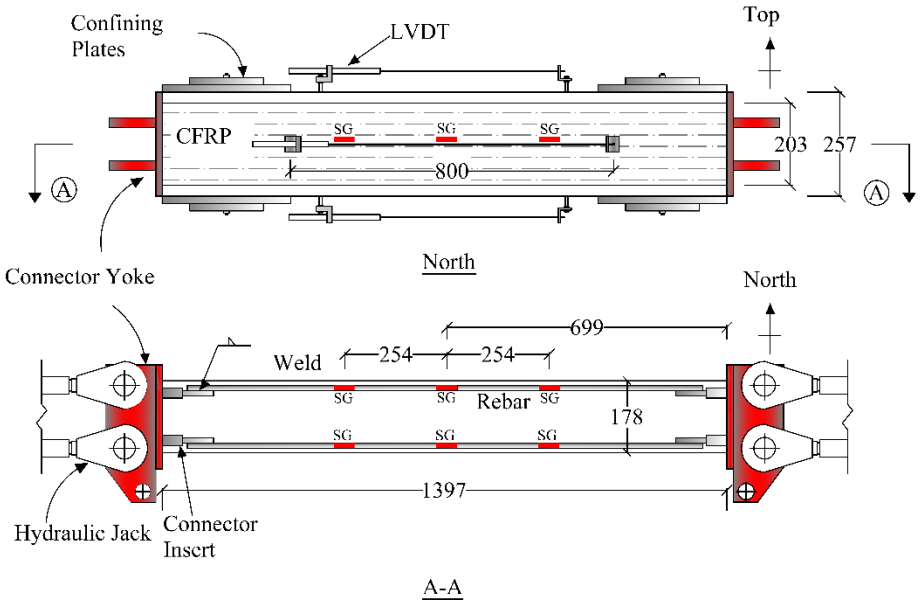

b) Specimen layout

Fig. 2. Test setup and specimen layout (units in mm)

Table 1
Material properties.

Material				
Steel		#3	#4	#5
	f_y, (MPa)	458	462	469
	E_s, (GPa)	189	190	195
FRP		SCH-11UP	SCH-41S	
	t, (mm)	0.6	1.0	
	$F_{u,FRP}$, (MPa)	827	876	
	E_f, (GPa)	83	72	

Table 2
Geometric and strengthening characteristics of the specimens [35].

Specimen	Ø (mm)	ρ_S *(%)*	ρ_f (%)	ρ_{eff} (%)	Wrapping Scheme	Anchorage method
REF_R3	0.375	0.31	-	0.058	-	-
REF_R4	0.5	0.55	-	0.049	-	-
REF_R5	0.625	0.87	-	0.045	-	-
S3-025-FA	0.375	0.31	0.56	0.04	U-Wrap	FRP anchor
S3-040-FA	0.375	0.31	0.90	0.035	U-Wrap	FRP anchor
S4-025-FA	0.5	0.55	0.56	0.04	U-Wrap	FRP anchor
S4-040-FA	0.5	0.55	0.90	0.04	U-Wrap	FRP anchor
S4-025-FW	0.5	0.55	0.56	0.045	Fully Wrapped	-
S4-040-FW	0.5	0.55	0.90	0.045	Fully Wrapped	-
S4-025-SB	0.5	0.55	0.56	0.039	Side Bond	-
S4-04-SB	0.5	0.55	0.90	0.058	Side Bond	-
S5-025-FA	0.625	0.87	0.56	0.049	U-Wrap	FRP anchor
S5-040-FA	0.625	0.87	0.90	0.045	U-Wrap	FRP anchor

The specimens are identified by steel rebar sizes Nos. 3, 4, and 5), FRP sheet thicknesses [0.6 and 1 mm (0.025 and 0.040 in.)], and wrapping schemes (Fully Wrapped, Side Bond, and U-wrap with FRP Anchor). As an example: "S4-040-FW" stands for the specimen with No. 4 rebar, 1 mm (0.040 in.) thick FRP sheets and Fully Wrapped (FW) wrapping scheme method. REF-R3, REF-R4, and REF-R5 stand for RC reference specimens with Nos. 3, 4, and 5 rebars, respectively.

For the test procedure, load control was first used until the cracks occurs, after that the displacement control mode was used until the failure of the specimen. In the loading control mode, tensile load was applied at increments of 2.2 kN/jack/min. For the displacement control steps in the post-cracking stage, the increment of the strain was set to 0.0001 (mm/mm)/min.

4. Digital Image Correlation Measurement Technique

Digital image correlation is an optical, non-contact based measurement method, which 3D displacements and deformations of a specimen are measured. DIC systems are well known techniques for non-contact full field measurement of deformations and strains. The basic principle consists of matching pixels between the initial and deformed images. The fundamental correlation function, C, which is a function of the coordinates of the reference image, defines the relationship of the reference image and the deformed image (Eq.13). The displacements in both directions are defined as u and v, and I is the reference image and is a function of the pixel values $x+i$ and $y+j$. I^* represents the image after deformation and is a function of the pixel values with the deformations applied. The correlation functions C, is the sum of the squared differences between the reference image and the deformed image, where the function is summed over the

subset size *n*. The measured subset is defined as a small area which contains points being tracked by the correlation function [36].

$$C(x,y,u,v)=\sum_{i,j=-n/2}^{n/2}\left(I(x+i,y+j)-I^{*}(x+u+i,y+v+j)\right)^{2}$$

(13)

A random pattern is first applied on the surface of the measuring object by spray paint or airbrush, similar to the example shown in Fig. 3. A suitable balance between the average black-white spots must be achieved in order to enhance the accuracy of the measurements. To capture a stereographic image of the test specimens in a 3D measurement, two cameras are used (Fig. 4). The size and location of measuring volume with respect to the cameras, the angle of cameras, and the position of the two cameras with respect to each other are first determined by system calibration. Calibration is performed by taking pictures of a calibration object, which has targets mounted on it with known sizes and distances to each other, through a set range of motions within the volume where the measurement is being captured.

Full field displacements of a specimen are captured by collecting digital images at pre-determined time intervals throughout the test and comparing the first image which represents the reference configuration with other images. By post processing the digital images, the ARAMIS DIC-3D software recognizes the structure of the stochastic pattern and allocates coordinates to image pixels [37]. The displacement field is measured through overlapping image details (or facets) which have a certain size, defined across the region of interest. A facet is used because it has a wider variation in gray levels which can be uniquely identified from other facets in the deformed image [23]. In Fig.3, a facet assigned to a digital image is shown. The deformation of the facet after several steps in testing is shown with respect to the reference image. Typically

increasing the facet size enhances the accuracy of the measurements but will lower the spatial resolution which is defined by the facet size [38].

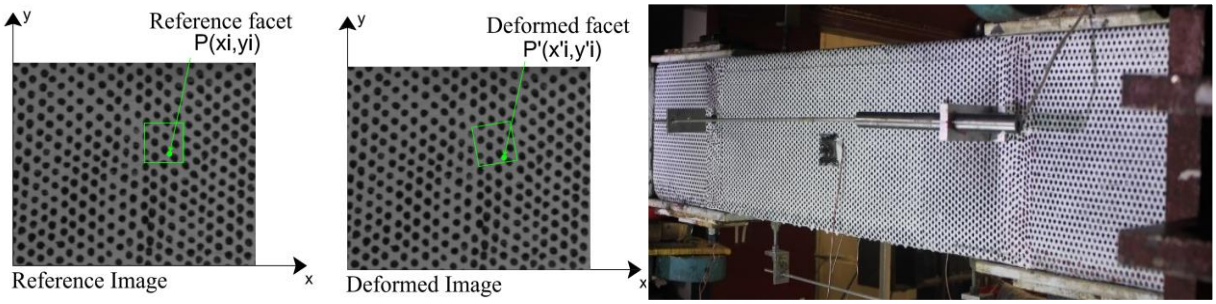

Fig. 3. The pattern on the surface of a concrete specimen and facets

To obtain a common 3-D coordinate between images, the corner points from both cameras are used and the 2-D coordinates of the same facet are determined.

In this study, the specimens were prepared by applying a speckle pattern as shown in Fig.3. A thin layer of white flat paint was first applied on the surface, followed by a distribution of black dots using spray paint. The ARAMIS DIC-3D software by GOM [37] was used in this work. In the test set-up, the DIC system was positioned facing the surface of the specimen (Fig.4). The measuring distance for all the tests was set about 80 inches. To focus the image on the specimen's surface, the aperture of the lens was first completely open and then during the test, to improve the depth of field the lens aperture was closed. The shutter time was set to 60 ms. Finally, to avoid over exposure and to have a uniform illumination of the measuring surface, the light source was adjusted.

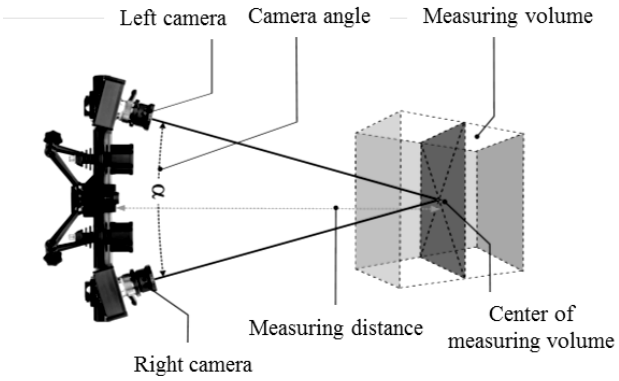

Fig.4. ARAMIS 3D sensor setup

In this study, a facet size of 19×19 pixels was chosen and the facet step was set to 15×15 pixels to avoid statistically correlated measurements. The crack characteristics including crack width, number of cracks, and spacing are monitored by using the ARAMIS system. In Fig. 5, the strain field in the direction of applied load (ε_x) of a specimen at a specific load level is shown using color gradient. The cracks are identified at locations with sudden increase in strain, ε_x. The crack widths are measured by assigning two points near the cracks and continuously measuring their distances.

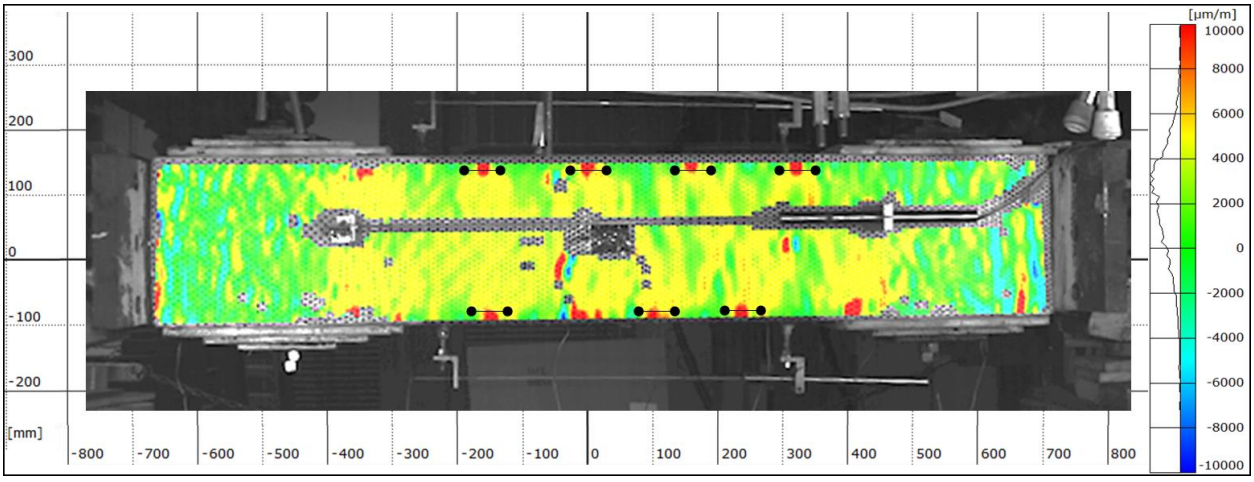

Fig. 5. Full strain field in the direction of applied load of a specimen at a specific load level

5. Test results and data analysis

In this section the experimental results of the uniaxial tensile tests of FRP strengthened RC specimens are presented. Details on the tensile behavior and cracking analysis of externally bonded FRP strengthened RC members are given.

5.1. Tensile behavior

The load- average strain curves (P-ε_m) of the tests are shown in Fig. 6. The average strain is calculated based on the measurements of LVDTs over the test region as shown in Fig. 2 (i.e., 800 mm).

The uniaxial tensile behavior of the FRP strengthened RC members can be defined by three different regions. The stress-average strain curve has an initial linear branch with steep slope, which corresponds to the un-cracked condition of the member (pre-cracking stage). After the first cracking, testing mode was switched to displacement control; therefore, the load dropped to accommodate the increase in strain due to cracking. Afterwards, the cracking stage begins and the slope of the stress-strain curve decreases due to progressive cracking in the FRP strengthened RC member. Finally, at the post-yielding stage, the crack development has been stabilized and the stress-strain curve increases monotonically until failure (Fig. 6).

Figs. 6a and 6b shows the results of the specimens with same steel and FRP reinforcement ratios but different wrapping scheme. It can be observed form Figs. 6a and 6b that the application of externally bonded FRP sheets significantly increases the capacity of the RC member. Also, the observed failure modes are debonding for specimen with side bond wrapping scheme, and FRP rupture for specimens with fully wrapped and U-wrap with FRP anchors. In both cases, the

average steel strain at failure is significantly smaller than that in RC members. Moreover, it can be observed that the specimens with fully wrapped and FRP anchors have a greater gain in capacity when compared to side bond wrapping scheme. This can be attributed to the fact that the failure mode for the side bond wrapping scheme is FRP debonding while the failure mode for fully wrapped and FRP anchors is FRP rupture. In the case of debonding, failure is experienced at a strain level which is lower than the ultimate strain of FRP, when the FRP separates form the concrete substrate. At these lower strain levels, the FRP is not able to utilize its full tensile capacity, effectively lowering the efficiency of the strengthening system. In the case of FRP rupture, the fibers reach their ultimate strain value and fracture at the point of maximum stress. Therefore, the effective strain for FRP rupture is highly greater than that of FRP debonding, which explains the greater gain in capacity.

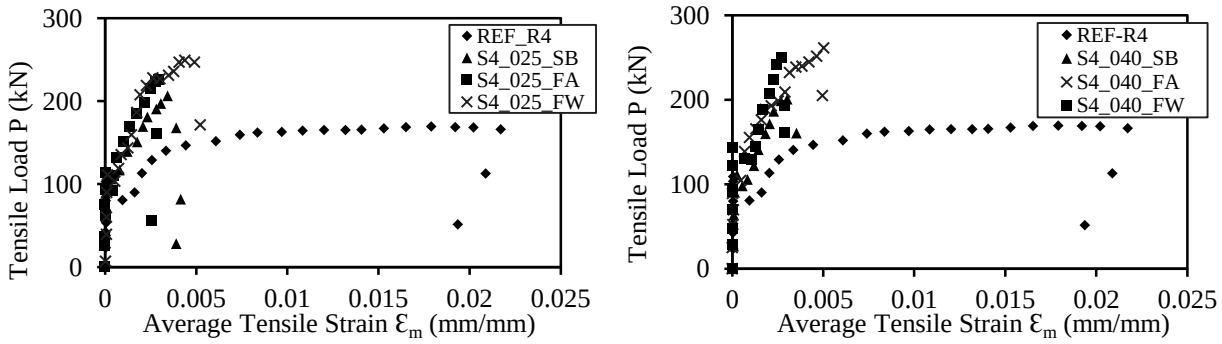

a) Specimen (ρ_s = 0.55%, ρ_f = 0.56%) b) Specimen (ρ_s = 0.55%, ρ_f = 0.90%)

Fig. 6. Experimental load-average strain curves

5.2. Tension stiffening effect

The tensile contribution of concrete, known as tension stiffening, is usually neglected when calculating the strength of RC members. However, tension stiffening affects the post-cracking stiffness and consequently the overall behavior in terms of deflection and crack width of the member under service load [39]. Tension-stiffening effect are useful in investigating the post-

cracking behavior of the FRP strengthened RC members and can provide additional information to explain the bond characteristics between the FRP and concrete interface, which is crucial for investigation of the crack width and crack spacing. If the tension stiffening effect is neglected, the calculated strains and deformations may be overestimated.

Fig. 7 shows the curves of normalized tensile stress of concrete with respect to the average tensile strain of tested specimens. The derivations of these curves are presented elsewhere [35]. Fig. 7a shows that the tension stiffening effect tends to be greater in the specimen with higher steel reinforcement ratio. With the increase in steel reinforcement ratio the bond characteristics between steel and the surrounding concrete increases and therefore influence cracking [34]. Fig. 7b indicates that compared with un-strengthened reference specimen (REF-R4), the specimen with FRP exhibited a greater tension stiffening effect. Also, when compared the specimen wrapping with different thickness of FRP sheets, it was found that the specimens strengthened with thinner FRP sheets (smaller FRP reinforcement ratio), tend to have a greater tension stiffening effect. It can be observed from Fig. 7c that that the tension stiffening is more evident in specimens strengthened using the fully wrapped and FRP anchor method compared to those using side bonding methods. The greater tension stiffening effect for the fully wrapped and FRP anchor can also be attributed to the greater performance of the bond action due to these wrapping methods.

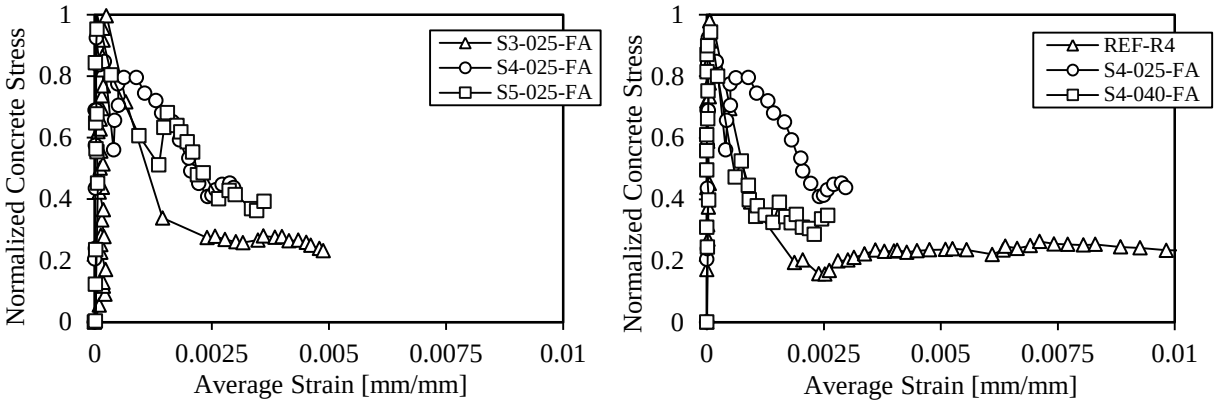

a) Specimen (ρ_f = 0.56%, FRP Anchors) b) Specimen (ρ_s = 0.55%, FRP Anchors)

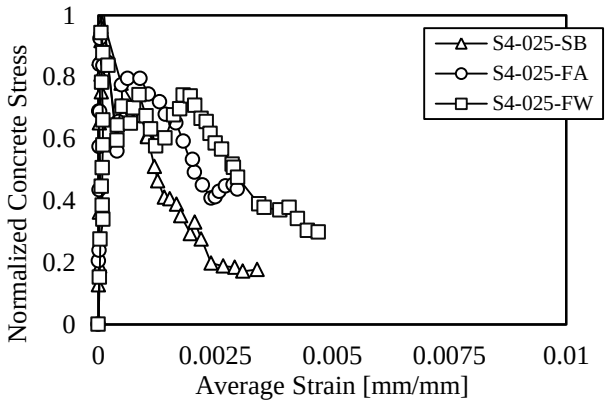

c) Specimen (ρ_s = 0.55%, ρ_f = 0.56%)

Fig. 7. Average stress-strain curves of concrete in tension

The contribution of the concrete in tension affects the stiffness of the FRP strengthened RC members after cracking. Therefore, the crack spacing and crack width are affected at service load level. Comparing the average stress-strain curves of concrete in tension for different specimens show that wrapping scheme and FRP reinforcement ratio affect the bond behavior of steel-concrete and also, FRP-concrete interface in FRP strengthened RC members. This will result in a different crack pattern in such members compared to RC members.

5.3 *Crack spacing*

5.3.1 Experimental results

The stabilized cracking phase is reached when the crack spacing between two existing cracks are too small for a new crack to develop in between. To determine the crack spacing, the cracks in the last phase of the test are considered since it is closest to the stabilized cracking. In Table 3 experimental measurements of the average crack spacing, S_{rm}, maximum crack spacing, $S_{r,max}$, and minimum crack spacing, $S_{r,min}$, are presented. The experimental average crack spacing is defined by the measurement of the spacing between the adjacent cracks along the length of the prism at different heights and averaging for the entire specimen at the stabilized cracking stage. The maximum and minimum crack spacing is defined based on the maximum and minimum measured crack spacing at the stabilized cracking stage throughout the specimen, respectively. In Fig.8 experimental values for the ratio $S_{r,max}/S_{rm}$, computed for each prism in the stabilized cracking phase is shown. The mean value of the ratio $S_{r,max}/S_{rm}$ and $S_{r,min}/S_{rm}$ are shown with a horizontal dashed lines. As mentioned before, EC2-04 [17] assumes a value of 1.7 for the ratio of the maximum to average crack spacing for RC structures; which is observed to be high compared to the experimental value of $S_{r,max}/S_{rm}$ equal 1.38 for FRP strengthened RC members.

Table 3
Experimental maximum, minimum and average crack spacing at stabilized cracking stage.

Specimen	No. of cracks	$S_{r,max}$ (mm)	$S_{r,min}$ (mm)	S_{rm} (mm)
REF_R3	3	281	218	250
REF_R4	4	305	167	234
REF_R5	4	257	188	236
S3-025-FA	7	169	57	119
S3-040-FA	9	146	82	111
S4-025-FA	8	145	88	113
S4-040-FA	8	165	79	111
S4-025-FW	8	161	87	107
S4-040-FW	7	188	50	111
S4-025-SB	7	178	88	122
S4-04-SB	5	280	78	171
S5-025-FA	6	199	76	146
S5-040-FA	6	174	118	134

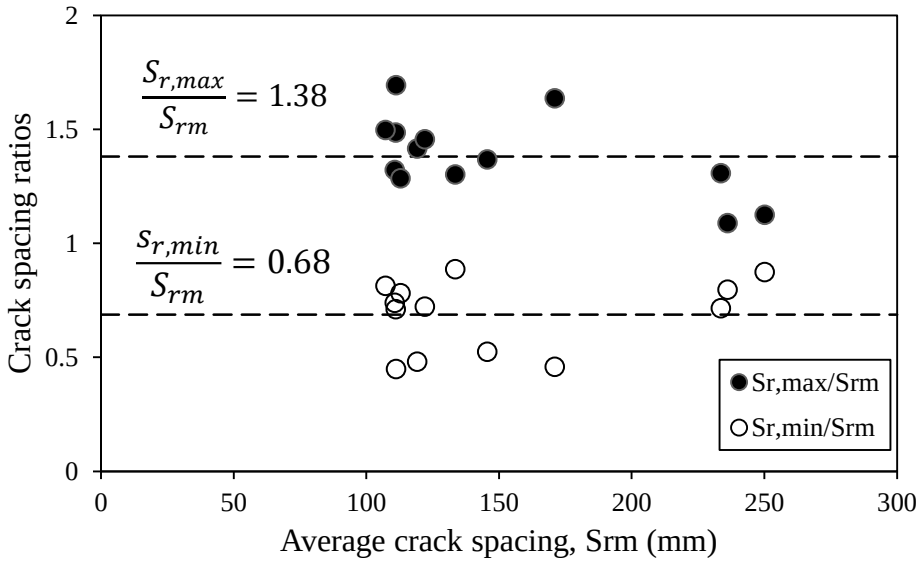

Fig.8. Ratios of maximum and minimum to average crack spacing vs. average crack spacing

5.3.2. Comparison with design provisions

The experimental results of the tests presented herein, and also the experimental data available in literature [4, 8, and 9] are used to review the effectiveness of the available design provisions discussed in section 2.1., for calculating the crack spacing in FRP strengthened RC members.

In Fig. 9, the experimental values of mean crack spacing, $S_{rm,exp}$, are compared with the design values provided by EC2-92 (Eq. 4), EC2-04 (Eq.6), and *fib*14 (Eq.8).

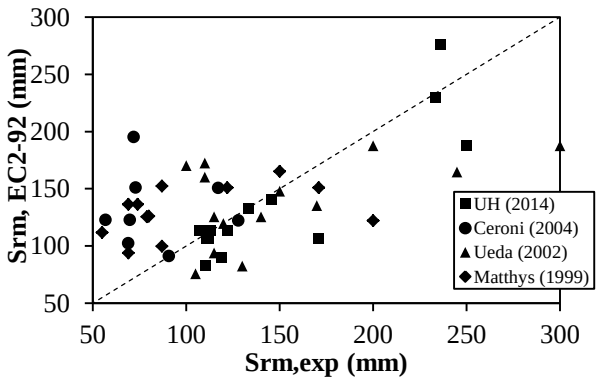

(a) EC2-92

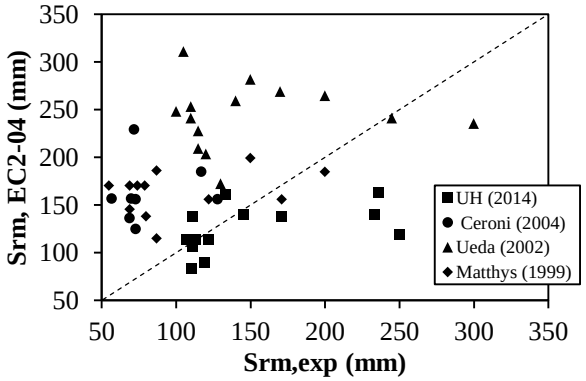

(b) EC2-04

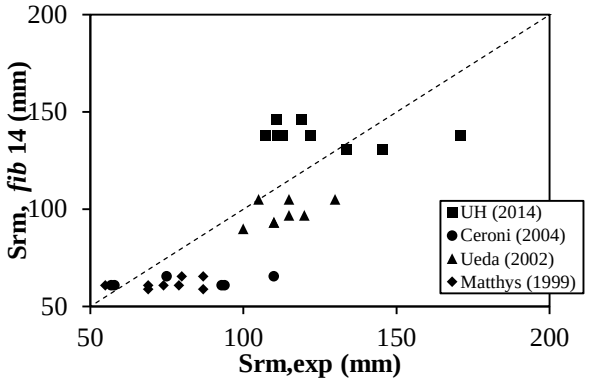

(c) *fib* 14

Fig.9. Experimental and code values of crack spacing (a) EC2-92, (b) EC2-04, (c) *fib* 14

In order to assess the suitability of the code predictions, for each approach examined, the mean percentage of deviation, $\sigma_{\%}$, of the code provisions with respect to experimental results are calculated as follows:

$$\sigma_{\%} = \sqrt{\frac{\sum_{i=1}^{n}\left(\frac{code_i - \exp_i}{\exp_i}\right)^2}{n-1}} \tag{14}$$

Where, $code_i$ is the code provisions corresponding to the experimental result, $\exp_i$, and n the total number of available experimental results used in the statistical analysis. Furthermore, the average ratio of code predictions to experimental results, δ, the standard deviation of variable δ, coefficient of determination, R^2, and correlation coefficient, r, are reported in Table 4. R^2 indicates how well the experimental results fit the prediction models. Correlation coefficient, r, is a measure of the degree of linear dependence between experimental results and the prediction models.

Table 4
Statistical parameters of the crack spacing for code guidelines and experimental results

	S_{rm} (EC2-92)	S_{rm} (EC2-04)	S_{rm} (FIB 14)	$S_{rm,An}$ (Eq. 15)
n	48	48	35	48
$\sigma_{\%}$	56	97.49	22.6	19.6
δ	1.21	1.63	0.97	1.01
σ_{δ}	0.52	0.74	0.22	0.20
R^2	-0.45	-1.27	0.65	0.87
r	0.57	-0.14	0.87	0.93

The statistical parameters reported in Table. 4 shows that for crack spacing the code guidelines of EC2-92 [16] and EC2-04 [17] presents a larger scatter compared to the *fib* 14 [21] prediction. The mean variable of parameter δ equal to 1.21 and 1.63 for EC2-92 and EC2-04 respectively, shows the over-estimation of the experimental results. As in *fib* 14, δ equals 0.97, which shows a good agreement between experimental results and the code predictions. Also, evaluating the R^2 and r values for *fib* 14 compared to EC2-92 and EC2-04 show that *fib* 14 predictions show a better agreement with the experimental results. The R^2 value for EC2-04 equals -1.27, which shows that the prediction are very scatter compared to EC2-92 and *fib* 14. In a previous research [35] the authors compared their experimental results with the code predictions, and it was found that the EC2-92 shows a better prediction of the results compared to the EC2-04 and *fib* 14 codes; This can be attributed to the fact that increasing the number of experimental test used in the statistical analysis will result in a more precise analysis of the crack spacing predictions. Also, the experimental results presented by Ueda et al. [9] showed a good agreement with the *fib* 14 code formulas, compared to the other experimental tests in the database.

The comparison of code predictions and experimental results for crack spacing in FRP strengthened RC members highlights the need for further investigations and

development of new formulations to accurately predict the crack spacing in FRP strengthened RC members.

5.3.3 New proposed formula

The experimental database which consists of the tests performed by the authors and also the available experimental results in literature [4, 8, and 9] was used to calibrate a new formula for predicting the cracks spacing in externally bonded FRP strengthened RC members. The same approach used in EC2-04 [17] for calculating crack width and spacing was adopted. Based on previous research studies, the main parameters influencing the cracking phenomena such as rebar diameter, effective area of concrete, concrete cover, FRP reinforcement ratios, and parameters such as wrapping scheme was considered in the development of the new formula. The following expression is proposed for the crack spacing prediction in FRP strengthened RC members:

$$S_{rm,An} = 2.54c + 0.016^{k} \frac{A_{c,eff} d_b^{1.97}}{A_s + A_f \left(\frac{E_f}{E_s} \right)^{24}} \quad (15)$$

Where, c is the concrete cover, $A_{c,eff}$ is the effective area of concrete, d_b is the rebar diameter, A_s and A_f are the area of rebar and FRP, respectively, E_s and E_f are the Young's modulus of elasticity of steel and FRP, respectively. The variable *k* considers the effect of wrapping scheme on the crack spacing. In the case of fully wrapped method and U-wrap with FRP anchor, k=1.0, and side bonding, k=0.95. In order to use this formulation for crack spacing in RC members, the k factor is to be 0.9 in such members.

The comparison considered between the experimental data base and the proposed model in Eq.

(15) is shown in Fig. 10. The statistical parameters reported in Table. 4 shows that the mean percentages of deviation and the average ratio of code predictions to experimental results for the proposed equation have reduced compared to EC2-92 [Eq. (4)], EC2-04 [Eq. (6)] and also, *fib* 14 [Eq. (8)]. The variable δ and the standard deviation of variable δ are computed as 1.01 and 0.20, respectively; which show a better prediction compared to the code formulations.

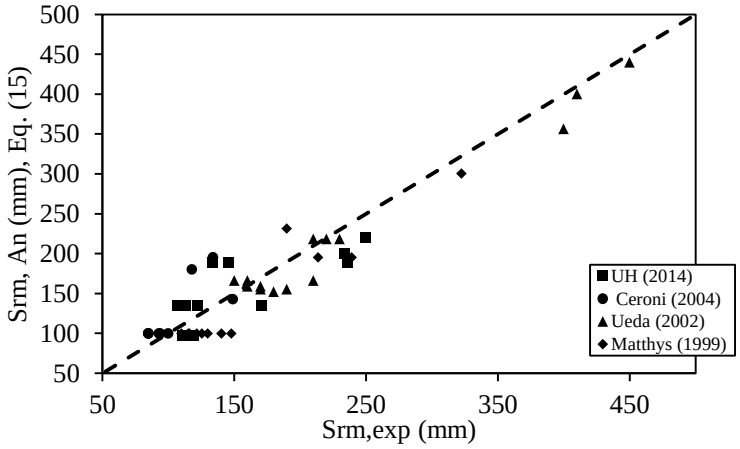

Fig. 10. Experimental vs. theoretical values of crack spacing proposed by authors [Eq. (15)]

5.4. Crack width

5.4.1 Experimental results

Crack width measurements obtained using the DIC system is presented in this section. Using the DIC system the crack widths were measured continuously during the test. It was observed that in FRP strengthened RC members; average crack widths were generally smaller than for un-strengthened members at the same smeared strain level [Fig. 11(a)], due to the additional bond action developing at the FRP-concrete interface which reduces the crack spacing [1, 32]. As shown in Fig. 11a, fully wrapped and U-wrap with FRP anchor wrapping schemes provide better control of crack width as compared to side bonding.

Furthermore, the thinner FRP (0.6 mm) provides better crack control compared to the thicker FRP (1.0 mm). It can be concluded that the fully wrapped method with thinner FRP shows a better behavior in terms of crack control compared to the other wrapping schemes and FRP thicknesses. This can be attributed to the greater tension stiffening effect in members strengthened with thinner FRP, which results in an increase in the bond between FRP and the concrete substrate and thereby decrease in crack width. The additional bond stress between the FRP and the concrete substrate in strengthened RC members result in the increase of the tension stiffening compared with that of the un-strengthened RC members; when the amount of FRP reinforcement increased, it was observed in the tests that the crack spacing decreased, which caused a greater deterioration of the steel bond. This deterioration became dominant and caused a decrease in the tension stiffening of the concrete and therefore, increase in crack width compared to members strengthened with thinner FRP. Fig.11 (b), shows that with the application of FRP sheets, the internal reinforcement ratio is not dominant in controlling the crack width in the U-wrap with FRP anchor wrapping scheme.

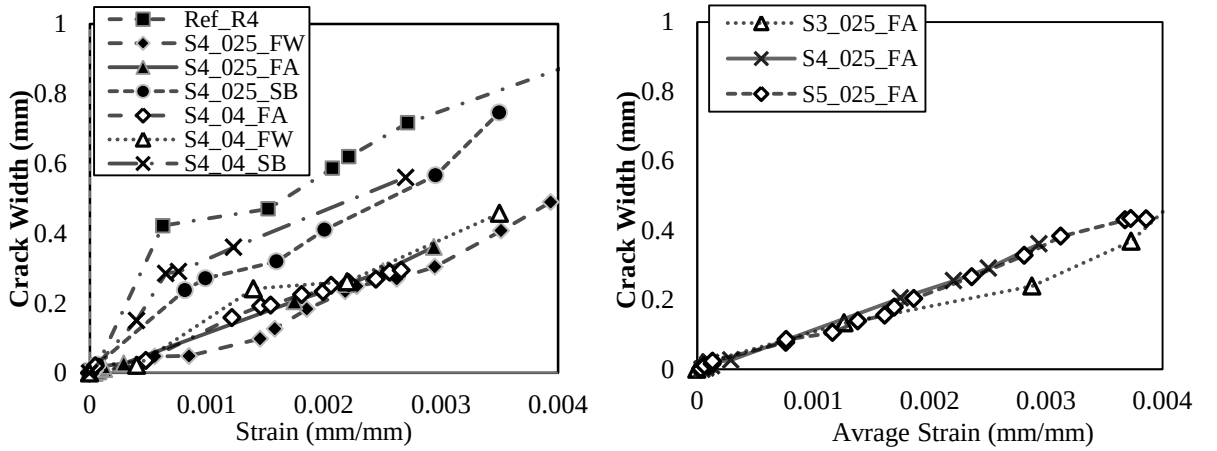

a) Specimen (ρ_s = 0.55%, ρ_f = 0.56%) b) Specimen (ρ_f = 0.56%, FRP Anchors)

Fig. 11. Relationship between average crack width and average strain (a) effect of

wrapping scheme, (b) effect of internal steel reinforcement

The first crack will form when the cracking load has been reached. Due to increment of applied load progressive formation of new cracks was observed and a combination of transverse and splitting cracks took place. Once the stabilized cracking stage was reached, no more new crack was developed and only the opening of existing cracks was observed. In Fig. 12, the final crack patterns at the stabilized cracking phase of three specimens are shown; an un-strengthened specimen (REF-R3), and two strengthened specimens with different FRP reinforcement ratios (S3-025-FA and S3-040-FA). It can be observed that applying externally bonded FRP results in increase in number of cracks, decrease in crack spacing and therefore decrease in crack width. As shown in Fig. 12a, three main cracks formed at the stabilized cracking stage in specimen REF-R3. With the addition of FRP in specimen S3-025-FA (Fig. 12b), the number of cracks increased. As discussed earlier, this is due to the increase in the tension stiffening effect. Similar behavior was observed for the specimen S3-040-FA (Fig. 12c). In specimens strengthened with smaller amount of FRP, the bond stress between FRP and concrete substrate increases while the bond stress between steel and concrete decreases. The increase of the FRP bond is dominant, so the tension stiffening increases compared to un-strengthened RC elements; when the amount of FRP reinforcements increases, the crack spacing decreases, which causes a greater deterioration of steel bond. Therefore, the specimens strengthened with thinner FRP had a better control of crack widths.

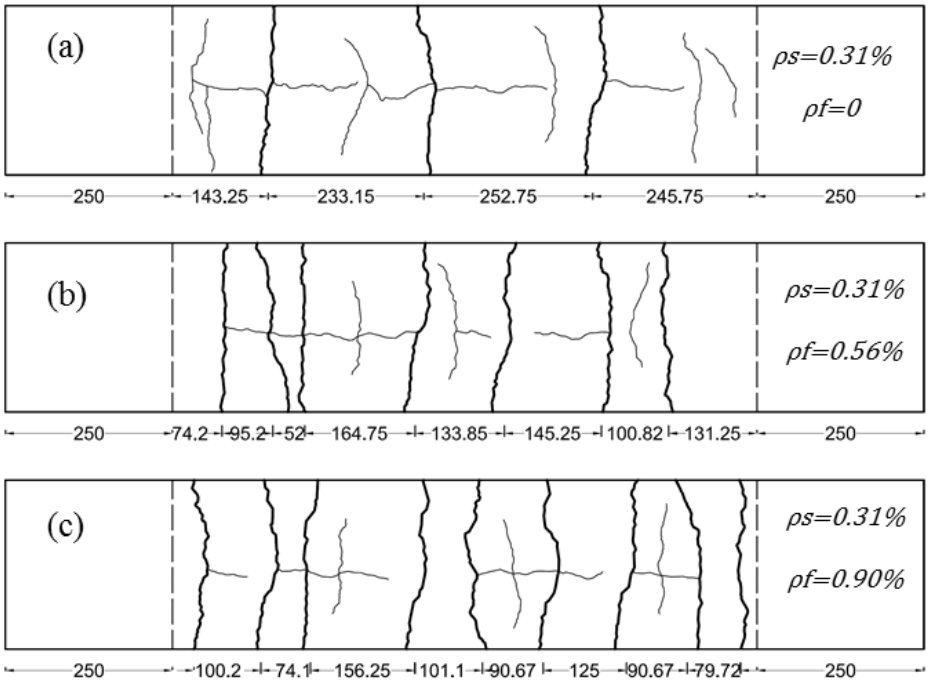

Fig. 12. Final crack pattern a) REF-R3, b) S3-025-FA, c) S3-040-FA (all dimensions in mm)

5.4.2. Comparison with design provisions

In order compare the experimental crack widths with the code predictions at serviceability conditions, a load stage of steel tensile stress equal to 400 MPa is considered for the evaluation. This assumption agrees with the commentary of Eurocode 2, where the database used to calibrate the code formula for crack width is made of results with steel stress ranging from 150 to 350 MPa [1]. In Fig. 13, the comparison between the experimental results in the database and code provisions is shown. Fig. 13a shows the comparison of experimental crack width results with EC2-92 [Eq. (2), Eq. (4), and Eq. (10)]. Fig. 13b shows the comparison of experimental crack width results with EC2-04 [Eq. (3), Eq. (6), and Eq. (11)]. Also, using Eq. (2), Eq. (8), Eq. (10) and, Eq. (12), the crack width prediction of *fib* 14 are calculated and compared with the experimental results (Fig.13c).

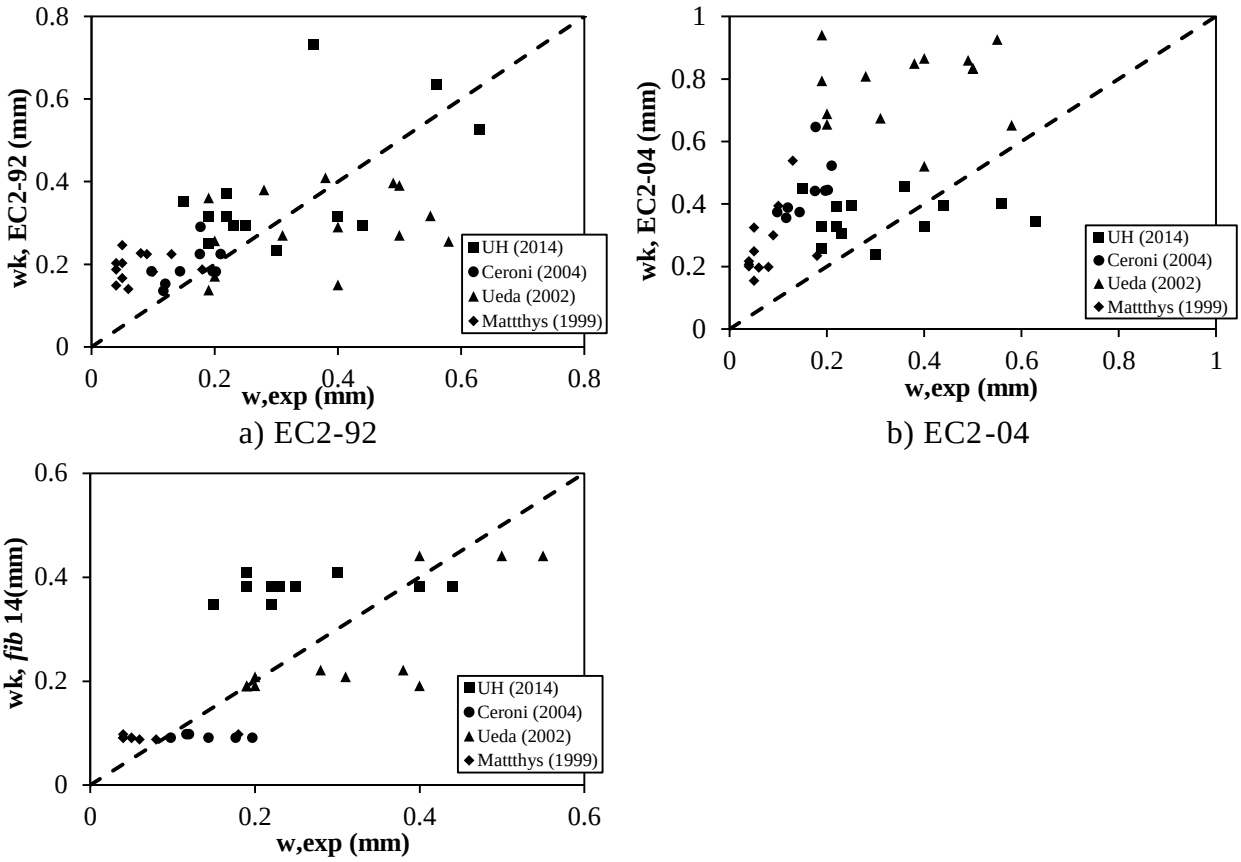

Fig.13. Experimental and code values of crack width (a) EC2-92, (b) EC2-04, (c) *fib* 14

In Table 5, the statistical summary of the experimental results and the code provision comparison are reported.

Table 5
Statistical parameters of the crack width, w_k, for code guidelines and experimental results

	w_k (EC2-92)	w_k (EC2-04)	w_k (*fib* 14)	$w_{k,An}$ [Eq. (13)]
n	48	48	35	48
$\sigma_{\%}$	132.34	214.76	64.42	45.96
δ	1.61	2.57	1.23	1.18
σ_{δ}	1.16	1.41	0.60	0.36
R^2	-0.19	-0.22	0.43	0.74
r	0.61	0.54	0.72	0.88

The statistical parameters reported in Table. 5 shows that same as the crack spacing, for crack width, w_k, the code guidelines of EC2-92 [16] and EC2-04 [17] presents a larger scatter

compared to the fib 14 [21] prediction. The mean variable of parameter δ equals to 1.61 and 2.57 for EC2-92 and EC2-04 respectively, shows the over-estimation of the predictions. As in fib 14, δ equals to 1.23, which shows a better agreement between experimental results and the code predictions. Also, evaluating the R^2 and r values for fib 14 compared to EC2-92 and EC2-04 show that fib 14 predictions show a better agreement with the experimental results. It is evident that the predictions of *fib* 14 which is specifically for FRP strengthened RC members, and uses the expression of average strain proposed in EC2-92 [16], shows a better accuracy compared to Eurocode 2 predictions. EC2-92 [16] Shows a better prediction compared to EC2-04 [17] (132.34% and 1.61 Compared to 214.76% and 2.57).

To calculate the average crack width using the proposed crack spacing equation [Eq. (15)], the approach suggested in EC2-04 [17] is used by introducing the proposed crack spacing, $S_{rm,An}$, in Eq. (3). The comparison between the experimental data base and the proposed crack width formulation, $w_{k,An}$, is shown in Fig. 14.

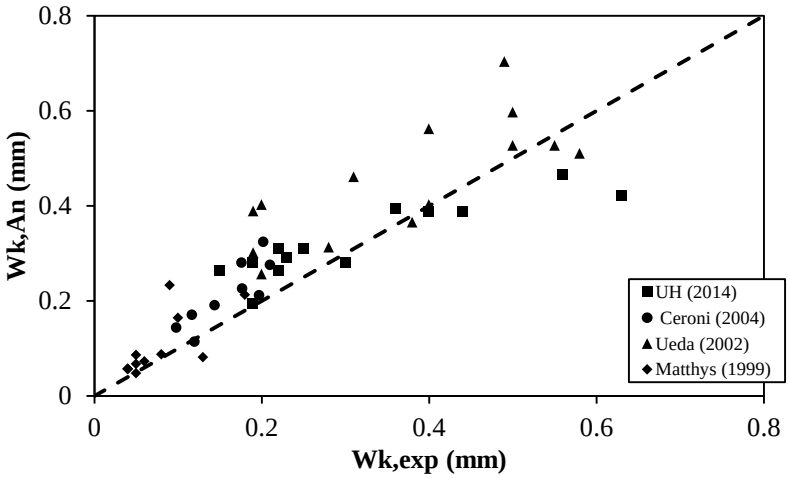

Fig. 14. Experimental vs. theoretical values of crack width proposed by authors [Eq. (3) and Eq. (15)]

The statistical parameters reported in Table. 5 show that the mean percentages of deviation and the average ratio of code predictions to experimental results for the analytical crack width equation have reduced compared to EC2-92 and EC2-04 crack width predictions. The variable δ and the standard deviation of variable δ are computed as 1.18 and 0.36, respectively; which show an improvement in crack width prediction compared to the Euro Code and *fib* 14 formulations.

6. Conclusions

The direct tension tests of externally bonded FRP strengthened RC prisms have been presented and discussed in this paper, focusing on crack spacing and widths. Crack control in FRP strengthened RC members is an important factor which must be considered for durability of the member. Same as RC members crack widths in FRP strengthened RC members should be limited in order to protect the steel reinforcement from corrosion.

The crack characteristics including crack width, number of cracks, and spacing are monitored by using the DIC system (ARAMIS) at the conducted experiments. With the use of the DIC system crack openings are monitored precisely and the crack width measurements are obtained continuously during the test. The DIC method has more accuracy and precision compared to visual observation and simple measurements for crack analysis.

At serviceability conditions the presence of the FRP sheets significantly affects the crack characteristics of RC members due to the additional contribution of the FRP by transferring tensile stresses to the concrete. Also, wrapping scheme was found to have a great impact on the crack characteristics of the FRP strengthened RC members in tension. The effectiveness of the Eurocode 2 formulations and *fib* 14 for crack spacing and crack width predictions are evaluated using statistical analysis of a database, including the direct tension tests

conducted by authors and several benchmark tests in literature. Application of Eurocode 2 provisions on crack spacing and crack width of FRP strengthened RC members clearly overestimates the experimental values. Euro code 2 provisions of crack spacing and width do not provide accurate results when applied to FRP strengthened RC tension members and clearly overestimates the experimental values. Crack spacing and width formulations in *fib*14 show better predictions compared to Eurocode 2 formulations.

The experimental database is used to propose a new formulation to evaluate crack spacing and crack width, considering all the affecting parameters in the cracking phenomena. A substantial improvement in the crack spacing and crack width prediction is obtained using the crack spacing formulation presented in this paper; a good agreement with experimental results and a clear statistical significance are attained.

ACKNOWLEDGEMENTS

This research was supported by the National Science Foundation, award number 1100930. Steel reinforcement and FRP materials are donation from GERDAU AMERISTEEL Co. and FYFE. Co., respectively. Their support is greatly acknowledged.

References

[1] Ceroni F, Pecce M. Design provisions for crack spacing and width in RC elements externally bonded with FRP. Compos Part B: Eng, 40(1) (2009), pp. 17-28.

[2] ACI Committee 440. Guide for the design and construction of externally bonded FRP systems for strengthening concrete structures. ACI 440.2R-08, Farmington Hills, MI: American Concrete Institute; 2008.

[3] Farah K, Sato Y. Uniaxial tension behavior of reinforced concrete members strengthened with carbon fiber sheets. J Compos Constr, 15(2) (2011), pp. 215-228.

[4] Ceroni F, Pecce M, Matthys S. Tension stiffening of reinforced concrete ties strengthened with externally bonded fiber-reinforced polymer sheets. J Compos Constr, 8(1) (2004), pp. 22-32.

[5] Sato Y, Shouji K, Ueda T, kahuta Y. Uniaxial tensile behavior of reinforced concrete elements strengthened by carbon fiber sheet. In: Proc, 4th international symposium on FRP reinforcement, (1999), p. 697-710.

[6] Yoshizawa H, Wu Z. Crack behavior of plain concrete and reinforced concrete members strengthened with carbon fiber sheets. In: Proc, 4th international symposium on FRP for reinforced concrete structures, (1999), p. 767-779.

[7] Tripi J, Bakis C, Boothby T, Nanni A. Deformation in concrete with external CFRP sheet Reinforcement. J Compos Constr, 4(2) (2000), pp. 85-94.

[8] Matthys S. Structural behavior and design of concrete members strengthened with externally bonded FRP reinforcement. Doctoral dissertation. Gent University, Belgium, (1999).

[9] Ueda T, Yamaguchi R, Shoji K, Sato Y. Study on behavior in tension of reinforced concrete members strengthened by carbon fiber sheet. J Compos Constr, 6(3) (2002), pp. 168-174.

[10] Lee Y, Boothby T, Bakis C, Nanni A. Slip modulus of FRP sheets boned to concrete. J Compos Constr, 3(4) (1999), pp. 161-167.

[11] Mias C, Torres L, Guadagnini B, Turon A. Short and long-term cracking behavior of GFRP reinforced concrete beams. Compos Part B: Eng, 77 (2015), pp. 223-231.

[12] Noel M, Soudki K. Estimation of the crack width and deformation of FRP-reinforced concrete flexural members with and without transverse shear reinforcement. Eng Struct, 59(2014), pp. 393–398.

[13] Elsanadedy H, Abbas H, Al-Salloum Y, and Almusallam T. Prediction of intermediate crack debonding strain of externally bonded FRP laminates in RC beams and one-way slabs. J Compos Constr,18(5) (2014), pp. 04014008-1-16.

[14] Pecce M, Manfredi G, Cosenza E. Experimental response and code models of GFRP RC beams in ultimate and serviceability conditions. J Compos Constr, 4(4) (2000), pp. 182-190.

[15] Baena M, Turon A, Torres Ll, Mias C. Experimental study and code predictions of fiber reinforced polymer reinforced concrete (FRP RC) tensile members. Compos Struct, 93(10) (2011), pp. 2511-2520.

[16] Eurocode 2. Eurocode: Design of concrete structures-part 1: general rules and rules for buildings, European Committee for Standardization, EN 1992-1-1, Brussels, (1992).

[17] Eurocode 2. Eurocode: Design of concrete structures-part 1: general rules and rules for buildings, European Committee for Standardization, EN 1992-1-1, Brussels, (2004).

[18] ACI Committee 318. Building code requirements for structural concrete and commentary. ACI 318R-05. Detroit, MI: American Concrete Institute, (2005).

[19] CSA. Design and construction of building components with fiber rereinforced polymers. CAN /CSA-806-12.Rexdale BD, ON: Canadian Standards Association, (2012).

[20] JSCE. Standard specification for concrete structures. Japan society of civil engineers. Tokyo, (2007).

[21] Fib (International Federation for Structural Concrete). Externally bonded FRP reinforcement for RC structures: Basis of design and safety concept. *FIB Bulletin 14*, Laussanne, (2001).

[22] Alam S, Lenormand T, Loukili A, Regoin P. Measuring crack width and spacing in reinforced concrete members. In: Proc, 7th International conference on Fracture Mechanics of Concrete and Concrete Structures. Korea, Seoul, (2010), p. 377-382.

[23] Gencturk B, Hossain K, Kapadia A, Labib E., Mo Y.-L. Use of digital image correlation technique in full-scale testing of prestressed concrete structures. Measurement, 47 (2014), pp. 505–515.

[24] Choi S, Shah S.P. Measurement of deformation on concrete subject to compression using image correlation. Exp Mech, 37(3) (1997), pp. 307–313.

[25] Hosseini F, Gencturk B, Lahpour S, Ibague Gil D. An experimental investigation of innovative bridge columns with engineered cementitious composites and Cu-Al-Mn super-elastic alloys. Smart Mater Struct, 24(8) (2015), 085029.

[26] ACI 224.2R-92. Cracking of concrete members in direct tension. ACI committee 224. Detroit (USA): American Concrete Institute, (1992).

[27] Champiri M D, Mousavizadegan S H, Moodi F. A decision support system for diagnosis of distress cause and repair in marine concrete structures. Comput Concr, 9(2) (2012), pp. 99–118.

[28] Champiri M D, Mousavizadegan S H, Moodi F. A fuzzy classification system for evaluating the health condition of marine concrete structures. J Adv Concr Technol, 10(3) (2012), pp. 95–109.

[29] Borosnyoi A, Balazs G. Models for flexural cracking in concrete: the state of the art. Structural concrete journal of the FIB, 6(2) (2005), pp. 53-62.

[30] Beeby A.W. The influence of parameter φ/ρeff on crack widths. Structural Concrete, 5(2) (2004), pp. 71–83.

[31] Farra B, Jaccoud J. Bond behavior, tension stiffening and crack prediction of high strength concrete. International conference: Bond in Concrete from research to practice, proceedings. Riga Technical University, (1992), p. 9.1-9.10.

[32] Ferr-Borges J. Cracking and deformability of reinforced concrete beams. IABSE Publications, Zurich, (1966), p. 75-95.

[33] CEB-FIP. Model code for concrete structures. Comite Euro-Internaional du Beton. Paris (France), (1990).

[34] Yang G, Zomorodian M, Belarbi A, Acun B. Tension stiffening of reinforced concrete shear elements strengthened with externally bonded FRP sheets. 37th IABSE Symposium Madrid. Madrid (Spain), (2014), p. 145-152.

[35] Yang G, Zomorodian M, Belarbi A, Ayoub A. Uniaxial Tensile Stress-Strain Relationships of RC Elements Strengthened with FRP Sheets. J Compos Constr, (2015), 10.1061/(ASCE)CC.1943-5614.0000639, 04015075.

[36] Jin T, Goo N, Woo S, Park H. Use of a digital image correlation technique for measuring the material properties of Beetle wing. J of Bionic Engineering, 6 (2009), pp. 224–231.

[37] GOM mbh. ARAMIS user manual-software. GOM optical measuring techniques. Braunschweig (Germany), (2011).

[38] Ghiassi B, Xavier J, Oliveira D, Lourenço P. Application of digital image correlation in investigating the bond between FRP and masonry. Compos Struct, 106 (2013), pp. 340-349.

[39] Bischoff P. Tension stiffening and cracking of steel fiber-reinforced concrete. J Mater Civ Eng, 15(2) (2003), pp. 174–182.